



# Exploring efficiency and regeneration of magnetic zeolite synthesized from coal fly ash for water treatment applications



Sofi Buzukashvili<sup>a</sup>, Roberto Sommerville<sup>b</sup>, Ozan Kökkiliç<sup>a</sup>, Philippe Ouzilleau<sup>a</sup>, Neil A. Rowson<sup>c</sup>, Kristian E. Waters<sup>a,\*</sup>

<sup>a</sup> Department of Mining and Materials Engineering, McGill University, Montreal, Quebec, H3A 0C5, Canada

<sup>b</sup> School of Metallurgy and Materials, College of Engineering and Physical Sciences, University of Birmingham, Edgbaston, Birmingham, B15 2SE, UK

<sup>c</sup> School of Chemical Engineering, College of Engineering and Physical Sciences, University of Birmingham, Edgbaston, Birmingham, B15 2TT, UK

## ARTICLE INFO

### Keywords:

Zeolites  
Magnetic zeolites  
Coal fly ash  
CFA  
Heavy metals  
Wastewater

## ABSTRACT

This study investigates novel synthetic magnetic zeolites from coal fly ash (CFA) and laboratory-grade LTA zeolite enhanced with nano magnetite particles for the remediation of heavy metal ions ( $Pb^{2+}$ ,  $Cu^{2+}$ ,  $Zn^{2+}$ ,  $Ni^{2+}$ ) from wastewater. Utilizing a continuous flow system with a laboratory scale Wet High Intensity Magnetic Separator (WHIMS), heavy metal removal and magnetic particles' recovery from the treated solution was investigated in a process that could be appropriate to real-world systems. The adsorption performance was investigated under various operational conditions, maintaining a consistent selectivity order of  $Pb > Cu > Zn > Ni$ , repeating the selectivity order found in previous study of magnetic CFA zeolite in batch systems. Moreover, magnetic CFA zeolite was shown to be a more effective adsorbent when compared to magnetic LTA zeolite. Thus, when tested in continuous flow system under selected conditions, magnetic CFA zeolite removed 63 % Pb, 37 % Cu, 13 % Zn, and 7 % Ni while magnetic LTA zeolite removed 25 % Pb, 16 % Cu, 6 % Zn, and 3 % Ni. Furthermore, treated solution that passed through WHIMS did not contain any zeolite particles, as they were successfully captured in the metal grid.

Additionally, regeneration of metal-laden magnetic zeolites through desorption experiments was investigated by enhancing the ion-exchange process using a saturated NaCl solution. The results indicated that Pb, Zn, and Ni ions were fully desorbed from magnetic zeolite, while approximately 70 % of the Cu remained to the sample. The Cu remained in the sample may be attributed to its partial adsorption onto the carbonized binder, a highly oxygenated graphenic structure, which does not readily release the adsorbed Cu ions. As these findings highlight the difference between adsorption and desorption selectivity order, further investigation into the topic would be beneficial.

This research underscores the operational advantages of using magnetic LTA and CFA zeolites in industrial water treatment applications, illustrating their high adsorption capacity and straightforward desorption processes.

## 1. Introduction

Industries generate significant volumes of polluted wastewater that requires treatment and management systems to minimize environmental harm and comply with legal standards [1–5]. The nature and volume of generated wastewater vary significantly across industries, largely depending on the specific type of processing involved [2,6]. The most common contaminants in industrial water include chemicals, heavy metals, organic constituents, soils, pesticides, pharmaceuticals, and

other industrial by-products [1,7–9]. Heavy metals are considered as one of the most dangerous groups of pollutants as they are toxic, carcinogenic and not biodegradable [9–11] and are typically defined as metals with a density exceeding  $5 \text{ g/cm}^3$ , including lead (Pb), zinc (Zn), copper (Cu), cadmium (Cd), mercury (Hg), nickel (Ni), chromium (Cr) and arsenic (As) [11–13]. Thus, it is essential to treat wastewater contaminated with heavy metal ions before releasing it into the environment [9,14,15]. Among the most hazardous industries that produce large volumes of wastewater contaminated by heavy metals are

\* Corresponding author.

E-mail address: [Kristian.waters@mcgill.ca](mailto:Kristian.waters@mcgill.ca) (K.E. Waters).

chemical, food and dairy, textile, petrochemical, and mining industries [9,15].

The growing concerns over heavy metal pollution and its effects on human health and the environment have accelerated the development of affordable and sustainable remediation technologies [16]. These technologies include membrane filtration, ion-exchange, adsorption, chemical precipitation, and electrocoagulation among others [7,10,16]. Finding resilient and easily available adsorbent materials capable of repeated adsorption and desorption with high efficiency is crucial for the economic viability of next-generation adsorbents. The focus of this work is on finding such an adsorbent for heavy metal remediation from wastewater, focusing on  $Pb^{2+}$ ,  $Cu^{2+}$ ,  $Zn^{2+}$  and  $Ni^{2+}$  ions, which are among the most common pollutants in mining wastewater.

Zeolites are a naturally occurring class of aluminosilicates extensively used as adsorbents of heavy metals due to their unique porous structure and high surface area [1,17]. Though natural zeolites are widely available, synthetic zeolites offer significant advantages as they can be tailored to have specific properties, offer better adsorption capacities, and have uniform size [18–20]. The most commonly used zeolite types include LTA, X, Y, USY and ZSM-5 [21]. LTA zeolite, or zeolite type A, investigated in this work, is characterized by the formula  $|Na_2^{+}(H_2O)_{27}|_8[Al_{12}Si_{12}O_{48}]_8$  [22]. LTA zeolite type does not occur naturally and must be synthesized [22]. Recently, significant attention has been focused on synthesizing zeolite from wastes and by-products, such as coal fly ash, rice husk, red mud, lithium slag among others, to address environmental issues and enhance waste management strategies, thereby promoting sustainable development [20,21,23,24].

In this work, coal fly ash (CFA) was used as a source of raw material for zeolite synthesis as it has previously been shown that CFA derived zeolites are effective adsorbents for removal of heavy metals from water [8]. CFA is a fine powder by-product of coal combustion, recognized as one of the most significant industrial wastes [25]. Despite the significant production of CFA, its global utilization rate remains relatively low, with a significant amount of the remaining ash being stored in landfills, ash ponds, surface impoundments, or stacked [25,26]. This disposal method poses serious environmental risks, contaminating soil, water sources, and air, thereby amplifying ecological and health issues associated with CFA management [25]. While the shift away from coal energy production is ongoing, some of the world's largest coal-dependent countries continue to operate coal-fired power plants [26,27]. This ongoing use, coupled with the extensive historical stockpiles of CFA, suggests that it will remain a significant environmental pollutant for the foreseeable future [27–30].

Although zeolites derived from coal fly ash (CFA) are effective for removing heavy metals from water, the issue of removing fine zeolite particles after treatment often persists [31,32]. To address this challenge, magnetic zeolite was synthesized in recent work by application of novel PVA solution method binding iron oxide ( $Fe_3O_4$ ) nanoparticles to zeolite [33,34]. Iron oxide nanoparticles possess superparamagnetic properties, high chemical stability, large surface area, high magnetic coercivity, and low toxicity and are often used to make a variety of magnetic adsorbents [31,35,36]. These properties allow iron oxide nanoparticles to be used as an adsorbent itself [37–39], however, the main problem remains the recycling of nanoparticles due to their size [40,41]. By binding iron oxide nanoparticles with zeolite, zeolite takes on iron oxide properties such as superparamagnetism, while remaining or even improving their adsorption capacity [33,34]. Furthermore, it was shown in previous research, that magnetic zeolite can be completely extracted from treated solutions in one cycle by feeding solution into wet high intensity magnetic separator (WHIMS) at 1.4 T [33,34].

In the present study, the performance of two magnetic zeolites is compared for the adsorption of  $Pb^{2+}$ ,  $Cu^{2+}$ ,  $Zn^{2+}$  and  $Ni^{2+}$  ions using a continuous flow experimental design. In this setup, the treated solution with magnetic zeolite particles is fed directly into WHIMS and then recirculated back into the water treatment cycle. Prior to their magnetic modification, both synthetic zeolites were characterized as type A

zeolites. First investigated zeolite (LTA-Z) was synthesized from analytical grade chemicals using a hydrothermal method [34], while the second (CFA-Z) was synthesized from CFA through microwave-assisted fusion followed by hydrothermal crystallization [33]. After their magnetic modification, magnetic zeolites were tested in continuous flow systems. Such experiments provide us a better understanding of magnetic zeolites adsorption behaviour under steady state that are common in industrial processes where adsorption is typically conducted continuously. Additionally, the data from these experiments provide the data on the dynamic behavior of adsorbents, that would help determine magnetic zeolites capacity in continuous system and the time it takes for it to become saturated, which are vital parameters for process optimization.

Furthermore, this work explores the regeneration of magnetic zeolite using a desorption method. Our previous studies have shown that the adsorption of metal ions onto the zeolites occurs through an ion exchange mechanism, where sodium ions in the zeolite are replaced by metal ions from the solution [33,34]. Leveraging this property, we reverse this process by inducing the exchange of metal ions in the zeolite for sodium ions from a saturated sodium chloride NaCl solution.

Finding a method for effective regeneration of metal laden zeolite and reusing it in further cycles of water treatment is crucial for economic and environmental considerations. Thus, this study aims to help in understanding of synthesized LTA and CFA magnetic zeolites adsorption efficiency in continuous flow application and improve their environmental impact.

## 2. Materials and methods

### 2.1. Zeolite synthesis

#### 2.1.1. LTA Zeolite synthesis

Linde Type A (LTA) zeolite (Si(50), Al(50)) was synthesized using the synthesis method described in *Verified Syntheses of Zeolitic Materials* [42]. For the synthesis, sodium hydroxide (Thermo Fisher Scientific Inc., Waltham, MA, USA, >99 % NaOH), sodium aluminate (Fisher Scientific, Na<sub>2</sub>O:Al<sub>2</sub>O<sub>3</sub>:3H<sub>2</sub>O), sodium metasilicate (Thermo Fisher Scientific Inc., Waltham, MA, USA, Na<sub>2</sub>SiO<sub>3</sub>:5H<sub>2</sub>O) and reverse osmosis (RO) water were used. For the detailed description of the synthesis process of LTA zeolite (LTAZ) used in this study, readers are referred to Buzukashvili et al. [34].

#### 2.1.2. CFA Zeolite synthesis

The CFA used in the zeolite synthesis was a byproduct of Rocktron's beneficiation process [43]: Pre-treated CFA was used as the feedstock for the zeolite synthesis process, which involved two stages: microwave-assisted fusion, and hydrothermal crystallization. For further details on the synthesis method of CFA-derived zeolite (CFAZ) used in this study readers are referred to Sommerville, 2017 [44].

Comparison of synthesis parameters between LTA and CFA zeolites can be found in Table 1 represented below.

#### 2.1.3. Magnetic zeolite synthesis

To render CFAZ and LTAZ magnetic, a novel method involving a high-temperature colloidal polyvinyl alcohol (PVA) solution to bind zeolite and magnetic nanoparticles together was used [33,34]. Zeolite fine powder was mixed with iron oxide nano-powder in a 10:0.1 wt ratio, followed by the addition of 20 mL of colloidal polyvinyl alcohol (PVA) solution. The mixture was then sonicated and diluted with ~50 mL deionized water to observe the formation of a hydrogel. The formed hydrogel was dried at 160 °C for 2 h to facilitate bonding between zeolite and iron oxide via PVA crosslinking. Subsequent heating in a muffle furnace was conducted at 400 °C for 2 h to cure and carbonize the PVA crosslinking. For a more detailed description of the synthesis of magnetic CFA and LTA zeolites used in this study readers are referred to Buzukashvili et al. [33,34], respectively.

**Table 1**

Comparison of synthesis parameters between LTA and CFA zeolites used in this study.

Parameter	LTAZ	CFAZ
Source Material	Analytical grade chemicals (sodium hydroxide, sodium aluminate, sodium metasilicate)	CFA, sodium aluminate, sodium chloride
Pretreatment	No	Yes (CFA was subjected to sink/float density separation, froth flotation, magnetic separation, size classification)
Synthesis methods	Hydrothermal	Microwave-assisted fusion, Hydrothermal method
Synthesis time & temperature	4 h at $99 \pm 1^\circ\text{C}$	2 h at $90^\circ\text{C}$ , then 3 h at $95^\circ\text{C}$
Synthesis vessel	Sealed polypropylene bottle	Conical flask stirred with magnetic stirrer
After synthesis procedure	Filtered, washed with deionized water, dried	Filtered, washed with distilled water, dried

## 2.2. Continuous flow experiments

For continuous flow system, the design that is schematically shown in Fig. 1 was employed. The process begins with contaminated solution pumped from Beaker 1 using Pump 1 into the Beaker 2. Here, magnetic zeolite particles are introduced, and a mechanical stirrer set at 400 rpm ensures thorough mixing. Simultaneously, the treated solution is pumped out from Beaker 2 by Pump 2 which is set to the same volumetric flow rate as Pump 1, such that the volume in Beaker 2 remains constant. Solution that is pumped from Beaker 2 will contain magnetic zeolite particles, so before discharge it is pumped directly through a lab scale wet high intensity magnetic separator (WHIMS) (Bunting Redditch, Redditch, UK) where the magnetic zeolite particles are trapped in the metal matrix due to the magnetic force acting on the particles. During these experiments WHIMS was operated at 12A and 184V generating a magnetic field of 1.4T.

After passing through the WHIMS, treated solution free of zeolite particles is collected into a Beaker 3 below WHIMS. Finally, based on the desired final metal ions concentration in solution, the solution from Beaker 3 can be either discharged or reintroduced for another cycle of water treatment with the addition of new magnetic zeolite by using Pump 3 to pump solution back into the cycle. Samples of solution are

taken over time from Beakers 1–3 to monitor the change of metal ion concentration over time. Experiments were repeated at different pump speeds and with a different amount of added zeolite and treated solution to investigate how the amount of zeolite and the retention time would affect the adsorption kinetics. All experiments were triplicated, and standard error of the mean was calculated for all the graphs shown in the Results section.

## 2.3. Batch adsorption and desorption experiments

### 2.3.1. Adsorption experiments

Adsorption experiments were carried out to investigate adsorption kinetics and quantify the adsorption capacity of the zeolites. Synthetic solutions containing  $\text{Cu}^{2+}$ ,  $\text{Zn}^{2+}$ ,  $\text{Ni}^{2+}$ ,  $\text{Pb}^{2+}$  ions were prepared using analytical reagent grade chemicals by preparing stock solutions which were then diluted using RO water to desired concentrations.  $\text{Cu}^{2+}$ ,  $\text{Zn}^{2+}$ ,  $\text{Ni}^{2+}$ ,  $\text{Pb}^{2+}$  solutions were prepared using Copper(II) nitrate trihydrate, 99 % (Thermo Fisher Scientific, U.S.A.), Zinc nitrate hexahydrate (98 % Thermo Fisher Scientific, U.S.A.), Nickel(II) nitrate hexahydrate (99 % Thermo Fisher Scientific, U.S.A.), and Lead(II) nitrate (99 % Thermo Fisher Scientific, U.S.A.), respectively. Tests were conducted with mixed-ions solutions where all four metal ions were present. The initial metal concentration of all investigated metal ions was 300 mg/L. Experiments were conducted at pH 5.5–6, at room temperature without temperature control and the stirring speed was set at 400 rpm. The pH of the solutions was measured before and after adsorption and no changes were observed. Thus, the decrease in concentration of metal ions were due to the adsorption by zeolite, rather than precipitation. A control experiment was conducted at the same pH where no zeolite was added. This resulted in no precipitation or change in metal concentration.

Unless otherwise stated, all adsorption experiments were conducted using 0.1 g zeolite in 100 mL of solution in 200 mL glass beakers positioned on an orbital shaker (New Brunswick Scientific Co., Canada) and covered with parafilm when using magnetic zeolite. Once the zeolite was introduced to the solution, periodic samples were taken from the solution using a syringe and filtered using 0.1  $\mu\text{m}$  filter (MilliporeSigma, Germany), stopping any further adsorption. Metals ion concentration of these filtered samples was measured using inductively coupled plasma optical emission spectroscopy (ICP-OES) using a Thermo Scientific iCAP 6000 series ICP Spectrometer (USA). Each experiment was conducted in triplicate and a control experiment with no addition of zeolite in solution was performed to confirm that there is no precipitation or change in

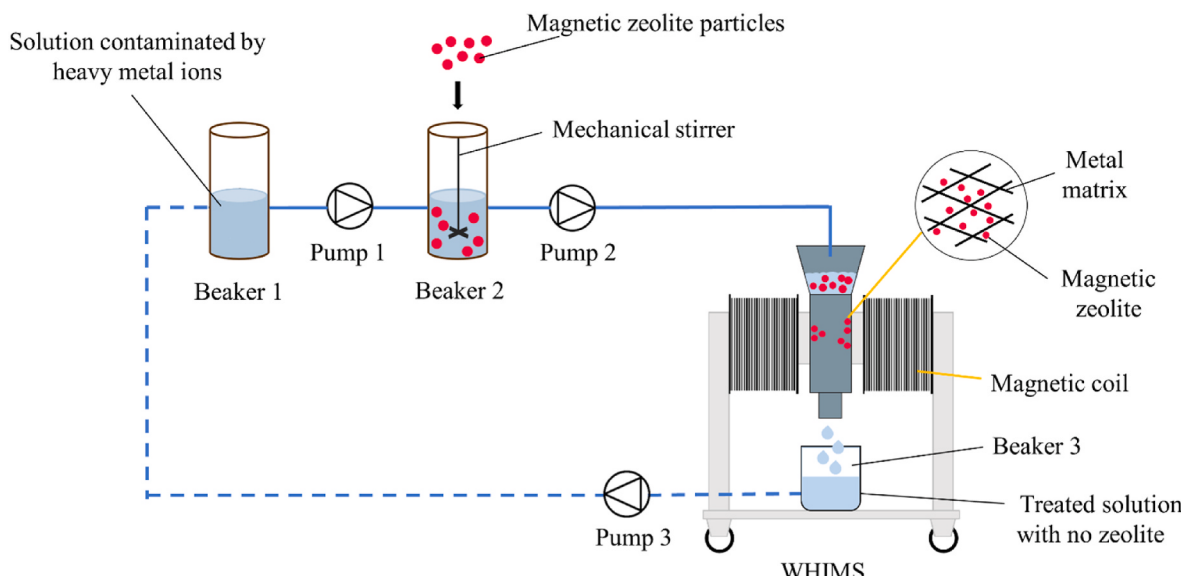


Fig. 1. Continuous flow design where treated solution goes directly into WHIMS.

metal concentration without zeolite in the system. The results are reported as average values with error bars denoting  $\pm 95\%$  confidence interval.

### 2.3.2. Desorption experiments

**Fig. 2** illustrates a schematic of metal ion (represented by the red colored spheres) desorption from magnetic zeolite (represented by the black colored spheres). The metal-laden zeolite is placed in a saturated NaCl solution that forces ion exchange to start.

To prepare saturated NaCl solutions, 36 g NaCl (anhydrous, Sigma-Aldrich, USA) was diluted in 100 mL RO (reverse osmosis) water. For desorption experiments, 100 mL of saturated NaCl solution was mixed with 0.1 g dried zeolite powder after the adsorption experiments and stirred using a mechanical stirrer at the room temperature. Samples were taken over time and analyzed using ICP-OES, to compare the concentration of metal ions in solution before and after desorption. Additionally, the zeolite was analyzed after adsorption and desorption experiments using SEM-EDS to compare the weight % of metals in the sample before and after desorption.

### 2.4. Characterization techniques

The zeolites were characterized via several techniques, including X-ray diffraction (XRD), Scanning electron microscopy (SEM), Energy-dispersive X-ray spectroscopy (EDS), Brunauer-Emmett-Teller (BET) technique, and particle size analysis (PSA).

XRD patterns were recorded using Bruker D2 phaser (Bruker, Germany) with the LYNXEYE XE-T, Cu, K $\alpha$ , ( $\lambda = 1.5418 \text{ \AA}$ ) X-ray source and operating conditions of 30 kV and 10 mA. The diffraction angle ( $2\theta$ ) was measured in the range of 5–70°. Diffraction patterns were analyzed using MAUD Java Program.

SEM was conducted using a SU3500 SEM (Hitachi, Japan) equipped with an 80 mm<sup>2</sup> X-MaxN Silicon Drift energy dispersive spectrometer (EDS) detector (Oxford Instruments, UK). The collected data were analyzed using AZtec software (Oxford Instruments, UK) to identify elements present in the samples.

PSA was performed using an LA-920 particle size analyzer (Horiba, Japan).

Specific surface area and adsorption average pore diameter were measured using the nitrogen Brunauer-Emmett-Teller (N<sub>2</sub>-BET) technique on a TriStar II Plus surface area and porosity analyzer (Micromeritics, U.S.A.).

Solution samples taken over time were analyzed by inductively

coupled plasma optical emission spectrometry (ICP-OES) using a Thermo Scientific iCAP 6000 series ICP Spectrometer (USA) to measure residual metal ion concentrations. Solution samples were diluted with 4% nitric acid prior to measurements.

## 3. Results

### 3.1. Zeolite characterization

LTAZ and CFAZ were characterized using XRD technique and compared to a reference spectra of LTA zeolite (type A zeolite) from the Database of Zeolite Structures [45] and are shown in **Fig. 3**. The results indicate that both LTAZ and CFAZ exhibit comparable intensities and peak positions to the reference LTA zeolite indicating that both zeolites are also type A or LTA zeolites.

After modification of zeolites into magnetic M-CFAZ and M-LTAZ, samples were analyzed using Scanning electron microscopy (SEM). The SEM images presented in **Fig. 4a** and b shows the morphology of zeolite samples at the scale of 10  $\mu\text{m}$ . As can be seen from the images, the particles are cubically shaped, which is common for zeolite type A [48–50], further confirming previous results from XRD analysis. Furthermore, the red areas shown in SEM-EDS images in **Fig. 4c** and d indicate the presence of Fe in the synthesized zeolites.

Additionally, **Fig. 4** demonstrates that the M-CFAZ (a) has a larger particle size compared to M-LTAZ (b) in the SEM-analyzed areas of the sample. To confirm these findings, particle size analysis (PSA) and surface area characterization (BET) were conducted. The results shown in **Table 2** further corroborate that M-CFAZ tends to have larger particles than M-LTAZ. The larger particle size of M-CFAZ contributes to its lower BET surface area, indicating that fewer adsorption sites are available per unit mass for adsorption compared to the smaller particles of M-LTAZ. This difference in particle size and surface area can influence the adsorption dynamics and capacity. The results shown in Section 3.2 show better adsorption performance of M-CFAZ. That could be attributed to the chemical composition and structural properties of M-CFAZ that may enhance its affinity for heavy metal ions. Additionally, the pore structure and distribution of M-CFAZ, even with a smaller surface area shown at the BET, might be more accessible to the targeted metal ions. These findings suggest that while surface area is an important parameter, other factors such as chemical composition and pore accessibility also play a significant role in determining the adsorption efficiency of magnetic zeolites.

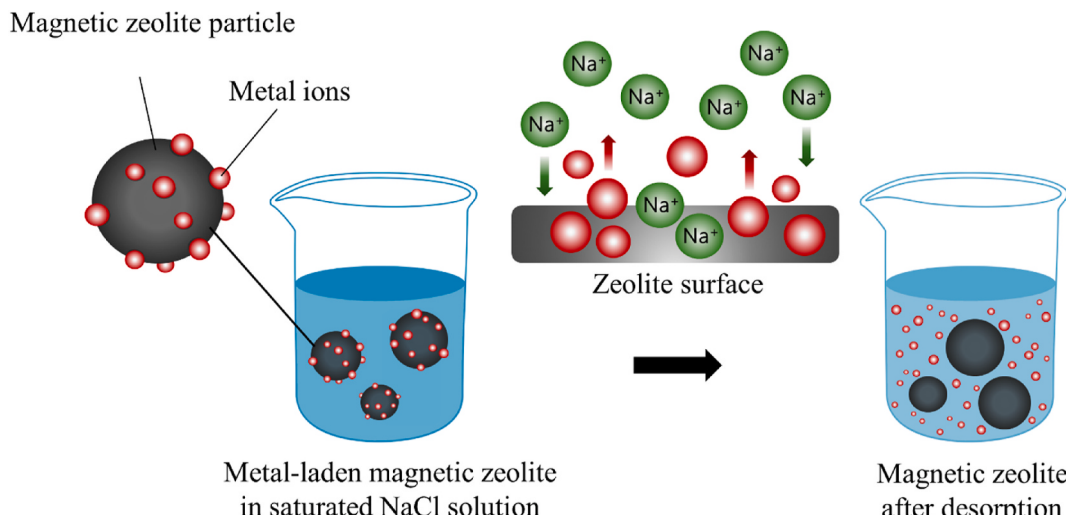


**Fig. 2.** Schematic illustration of desorption of metal ions ( $\text{Pb}^{2+}$ ,  $\text{Cu}^{2+}$ ,  $\text{Zn}^{2+}$  and  $\text{Ni}^{2+}$ ) from magnetic zeolite by to ion exchange with  $\text{Na}^+$  ions in saturated sodium chloride (NaCl) solution.

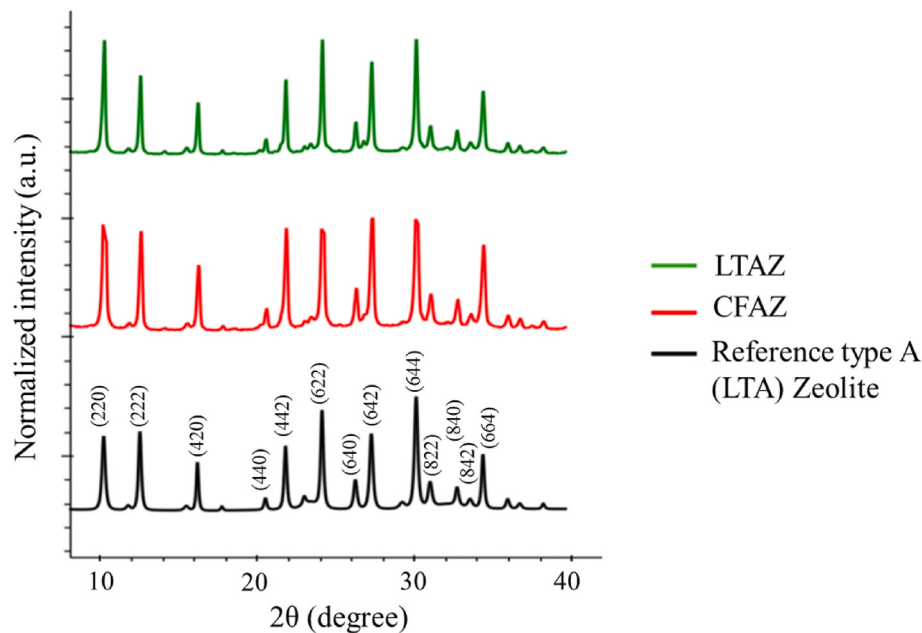


**Fig. 3.** XRD diffractograms of synthesized zeolites LTAZ and CFAZ compared with a reference XRD patterns of type A (LTA) zeolite [46,47].

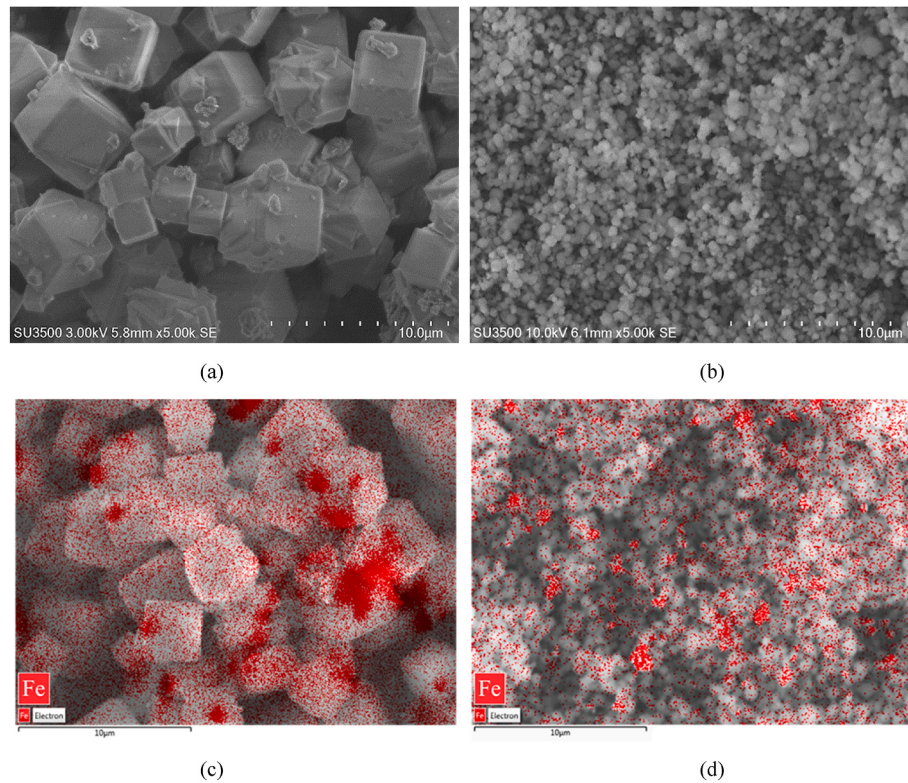


**Fig. 4.** SEM images of M-CFAZ (a) and M-LTAZ (b) and SEM-EDS images of M-CFAZ (c) and M-LTAZ (d) showing the presence of Fe (red areas) in the synthesized zeolites.

### 3.2. Adsorption experiments in continuous flow system

#### 3.2.1. M-LTAZ use at different flow rates

First, the adsorption performance of M-LTAZ in continuous flow system was compared at flow rates of 4 L/h (Experiment A) and 8 L/h (Experiment B). The parameters of Experiments A and B are summarized in Table 3 and the results are presented in Figs. 5 and 6. Fig. 5 illustrates the adsorption kinetics of investigated metal ions (Pb, Cu, Zn and Ni)

over time, with each metal represented by a distinct color. All experiments were conducted in triplicate and error bars on the graphs represent  $\pm 95\%$  confidence interval.

Fig. 5 illustrates the decrease of the metal ion concentrations over time for a flow speed of 4 L/h during 3 cycles of adsorption (a) and 8 L/h during 4 cycles of adsorption (b). The initial concentration of all ions in solution was 300 ppm in both cases. In Experiment A with a slower flow speed and longer retention time (40 min per cycle), after 3 cycles, the

**Table 2**  
Characterization of synthesized zeolites.

	Surface area, m <sup>2</sup> /g	Adsorption average pore diameter, Å	Particle size d <sub>90</sub> , μm
M-CFAZ	2.5	79	110
M-LTAZ	296	29	58

**Table 3**  
Parameters of the experiments with continuous flow with M-LTAZ.

Parameter	Value (Experiment A)	Value (Experiment B)
Zeolite dosage	1.5 g/L	1.5 g/L
Solution volume	3 L	3 L
Solution flow speed	4 L/h	8 L/h
Retention time	40 min	20 min
Number of cycles	3	4

final concentration of metal ions in solution was found to be 0 ppm for Pb, 35 ppm for Cu, 163 ppm for Zn and 209 ppm for Ni. Previous work on the use of magnetic zeolite synthesized from CFA used in adsorption of same metal ions in batch experiments [33] showed the following selectivity order of Pb > Cu > Zn > Ni, also indicating that metal ions

compete for the spots available on the zeolite surface. The observed order can be attributed to various factors, such as molecular size, molar weight, hydration radii, hydration enthalpies, cation solubility, pore size, and the quantity of exchangeable Na ions attached to the zeolite framework as detailed in Buzukashvili et al. [33]. The results observed in Fig. 5a show the same adsorption selectivity order. Based on these findings, it can be estimated that in the 4th cycle all Cu will be removed and more Zn than Ni will be adsorbed by M-LTAZ.

When comparing this with Experiment B (Fig. 5b), where flow rate was twice as fast (8 L/h) and therefore retention time was 20 min, even though the adsorption selectivity and kinetics pattern are similar to Experiment A, the kinetics and adsorption rate shown are different. Thus, after 4 cycles, the final concentration of metal ions in solution was found to be 0 ppm for Pb and Cu, 53 ppm for Zn and 174 ppm for Ni.

It can be seen from Fig. 5a and b that the effectiveness of the adsorption varies by metal, with efficient Pb and Cu removal within 3–4 cycles. The initial fast phase in the adsorption kinetics for all metals suggests a high affinity or of active sites in the zeolite at the beginning of the process, which decreases as these sites are occupied over time. Furthermore, the flow speed does not significantly affect adsorption kinetics as metal ions reached equilibrium after approximately 20 min at the slower flow rate (Fig. 5a). The differences observed between the two graphs underline the importance of optimizing adsorption conditions to enhance the removal efficiency of specific metal ions from solutions.

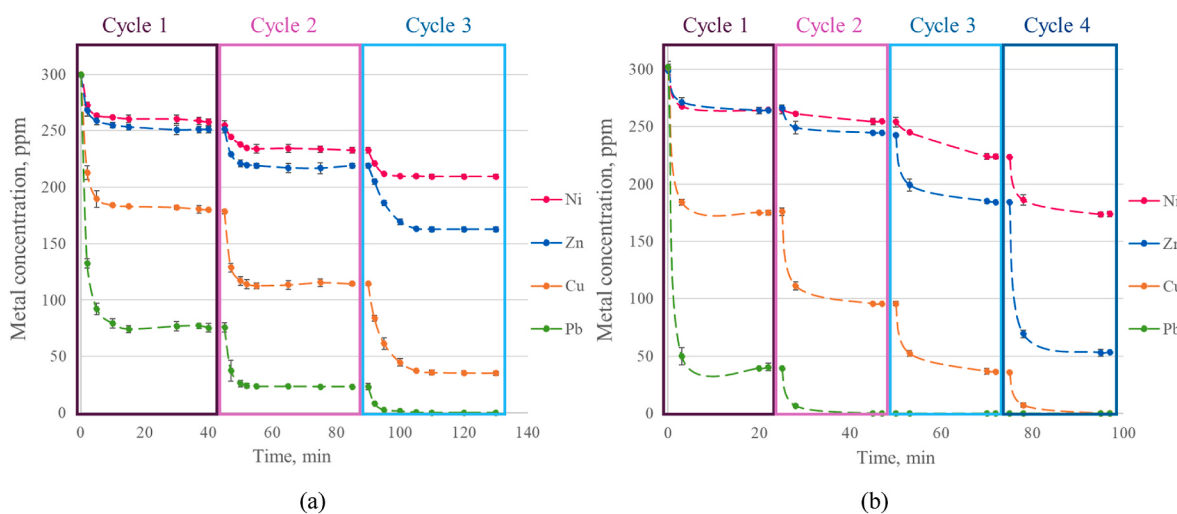


**Fig. 5.** Decrease of metal concentration in solution over time at a flow rate of 4 L/h (a) and 8 L/h (b) with M-LTAZ dosage of 1.5 g/L.

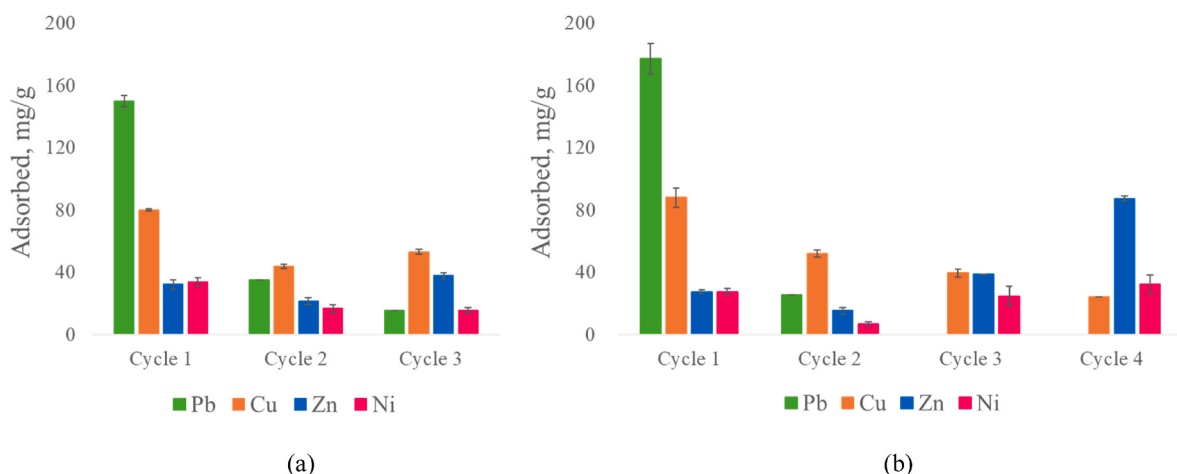


**Fig. 6.** The amount of adsorbed metal per cycle at a flow rate of 4 L/h (a) and 8 L/h (b) and M-LTAZ dosage of 1.5 g/L.

In the observed adsorption kinetics results, there is an inverse relationship between the adsorption of Pb ions and the other metal ions (Cu, Zn and Ni). This relationship can be attributed to competitive adsorption, where multiple metal ions in a solution compete for the limited available adsorption sites on the adsorbent.

The observed data suggest that when a significant amount of Pb is adsorbed, the adsorption of other metal ions such as Ni, Zn, and Cu is comparatively reduced within the same cycle. Conversely, when less Pb is adsorbed, there is an increase in the adsorption rates of Cu and other metals. This phenomenon can be explained by the competitive adsorption dynamics in multi-ion systems.

By using Equation (1) the adsorbed mass of metal per g of zeolite can be calculated for each metal during each cycle [51,52]:

$$Q = \frac{C_0 - C_e}{m} \times V \quad (1)$$

where Q is adsorption capacity (mg/g), V is solution volume (L), m is the adsorbent dosage (g),  $C_0$  and  $C_e$  are the initial concentrations of metal ions in solution and after the adsorption process, respectively (mg/L).

The results for both flow rates are represented in Fig. 6:

As can be seen for both investigated flow rates, in the 1st cycle the highest degree of adsorption is for Pb, followed by Cu, then smaller amounts of Zn and Ni following the selectivity order of Pb > Cu > Zn > Ni. While in the cycles 2 and 3, Cu is the most adsorbed metal (in absolute values), followed by Pb, Zn and Ni. Finally, in Fig. 6b, cycle 4, when there is no presence of Pb ions and lower amount of Cu ions were adsorbed due to their decreased concentration in solution, Zn removal increased significantly, along with the slight increase of Ni adsorption. This behaviour is expected to persist if more cycles are carried, with adsorption results changing due to the varying concentrations of metal ions in each cycle, however in accordance with the established selectivity order.

### 3.2.2. M-LTAZ and M-CFAZ comparison

To compare M-LTAZ and M-CFAZ adsorption performance in the continuous flow system with equivalent parameters, experiments with a flow speed of 8 L/h and zeolite dosage of 0.5 g/L were conducted. The lower dosage was chosen to investigate the adsorption capacity of zeolites. All parameters used in the experiments described in this section are provided in Table 4.

The results show significantly higher adsorption capacities for Pb across all cycles and followed by Cu, Zn and Ni. The pattern of metal adsorption of M-LTAZ (Fig. 7b) is similar to M-CFAZ, however, the overall adsorption capacities are generally lower compared to those in Fig. 7a. The consistency of the adsorption selectivity order of Pb > Cu > Zn > Ni in the continuous system aligns with that observed in batch systems for both M-CFA and M-LTA zeolites, which allows for further targeted adjustment of experimental design based on the desired quality of the treated water. For example, a larger amount of zeolite could be added to prioritize rapid Pb removal in the 1st cycle, while in subsequent cycles, a different amount or type of zeolite can be added to the system to target the removal of other metal ions. The results indicate that even small changes in experimental parameters affect the competition dynamics among the metal ions due to the complexity of the continuous

flow system and underline the influence of experimental conditions on the adsorption capacities and kinetics of different metals. These results can inform future studies aimed at optimizing adsorbent materials for the effective removal of specific metal ions from contaminated environments. The experimental data is summarized in Table 5.

### 3.3. Desorption

SEM-EDS analysis was performed on M-CFAZ and M-LTAZ after adsorption of heavy metal ions and after their subsequent desorption in NaCl solution. EDS scans of M-CFAZ (Fig. 8) and M-LTAZ (Fig. 9) show elements detected in the sample after desorption. Particularly, for both samples Al and Si are present (the main elements in zeolites), Na and Cl (due to the NaCl solution), Fe (indicates that the zeolite sample is still magnetic) and Cu (indicating that it was not desorbed completely from the sample). EDS analysis of the weight % of elements found in the sample was extracted from Aztec software and is presented in Fig. 10.

Both zeolites show the presence of all adsorbed metal ions after adsorption experiments as well as Fe, indicating that zeolite remains magnetic. However, after desorption experiments, only Cu of the adsorbed ions was detected in the sample, suggesting the complete desorption of Pb, Zn, and Ni. The results indicate that about 70 % of adsorbed Cu remained in the zeolite sample after desorption. Moreover, the results indicate minimal alteration of Fe, which implies that the magnetic properties of the zeolite were retained.

To confirm these results, samples were taken from solution during adsorption and desorption experiments and the metal ion concentrations were measured using ICP-OES. Fig. 11 shows adsorption (a) and desorption (b) kinetics of Pb, Cu, Zn and Ni ions per g M-CFAZ calculated using Equation (1). Fig. 12 shows the results of the same experiments using M-LTAZ. The pseudo-first-order, pseudo-second-order, Elovich, and intra-particle diffusion models were evaluated for fitting the experimental data [53–55]. The results demonstrated that the pseudo-second-order model provided the best fit for both adsorption and desorption experiments Equations (2) and (3) were used to generate the model plots, represented as dashed lines in Figs. 11 and 12.

$$\frac{dq_{ta}}{dt} = k_a(q_{ea} - q_{ta}) \quad (2)$$

$$\frac{dq_{td}}{dt} = -k_d(q_{td} - q_{ed}) \quad (3)$$

where  $k$  is the rate constant of the pseudo-second-order adsorption (g/mg·min),  $q_e$  is the adsorption capacity of the adsorbent at equilibrium (mg/g),  $q_t$  is the adsorption capacity of the adsorbent at time  $t$  (mg/g). The subscripts  $a$  and  $d$  refer to the adsorption and desorption processes, respectively.

The deviation of the experimental data from a perfect fit to the kinetic models can be attributed to the complexity of the mixed-ion solution system. In such systems, multiple factors influence adsorption and desorption processes, including competitive interactions between ions for active sites on the adsorbent, variability in ionic sizes and charges, and differences in affinities of the ions for the adsorbent surface.

For ease of comparison, the amount of adsorbed and desorbed metal ions is shown for both zeolites in Fig. 13 and the results are compared in Table 6.

The results of Figs. 11–13 show that both zeolites show high affinity for Pb and Cu adsorption and follow the selectivity order of adsorption Pb > Cu > Zn > Ni. This order is consistent with the order discussed in section 3.2 on continuous flow and aligns with previous work using M-CFAZ in batch adsorption experiments, which aligned best with the Langmuir linear adsorption model [33]. However, in the desorption experiments, both the kinetics and the amount of desorbed metal ions are in the order of Pb, Zn, Ni > Cu. Fig. 13 demonstrates that the same amounts of Pb, Zn, and Ni that were adsorbed by the zeolite were subsequently desorbed. Whereas only 15 mg/g of Cu was desorbed from

**Table 4**

Parameters of the experiment with continuous flow comparing performance of M-CFAZ and M-LTAZ with the identical parameters.

Parameter	Value
Zeolite dosage	0.5 g/L
Solution volume	1 L
Solution flow speed	8 L/h
Retention time	7.5 min
Number of cycles	5

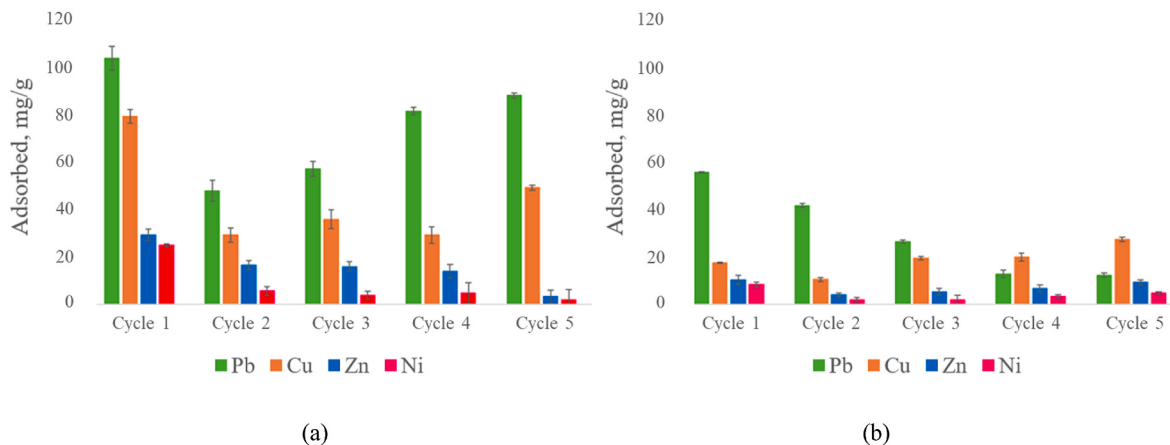


**Fig. 7.** The amount of adsorbed metal per cycle at a flow rate of 8 L/h and zeolite dosage of 0.5 g/L by M-CFA zeolite (a) and M-LTA zeolite (b). The results are presented over five cycles.

**Table 5**

Average amount of adsorbed metal per cycle by M-CFA zeolite and M-LTA zeolite at a flow rate of 8 L/h and zeolite dosage of 0.5 g/L.

Cycle number	Adsorbed, mg/g							
	M-CFAZ				M-LTAZ			
	Pb	Cu	Zn	Ni	Pb	Cu	Zn	Ni
1	104	79	29	25	56	18	10	8
2	48	29	17	6	42	11	4	2
3	57	36	16	4	27	20	5	2
4	82	29	14	5	13	20	7	3
5	88	49	3	2	12	27	9	5

both zeolites, indicating that about 70 % of Cu remained in the zeolite. These results further confirm SEM-EDS results shown in Figs. 8–10.

For calculating the desorption ratio of metal ions and comparing the desorption efficiency from M-CFAZ and M-LTAZ Equation (4) was used [56]:

$$D = \frac{q_d}{q_t} \times 100\% \quad (4)$$

where  $D$  is the desorption ratio (%),  $q_d$  is the amount of metal desorbed per unit mass of desorbing (mg/g), and  $q_t$  is the amount of metal adsorbed onto the mineral per unit mass of adsorbent at equilibrium (mg/g).

Using Equation (4), desorption ratio for M-CFA zeolite was

calculated as 100 % for Pb, 99 % for Zn, 97 % for Ni and 29 % for Cu; for M-LTA zeolite, desorption ratio was found as 100 % for Pb and Ni, 99 % for Zn and 31 % for Cu. These results are summarized in Fig. 14.

The results confirm the findings shown in Figs. 8–10, and indicate that during desorption experiments Pb, Zn and Ni ions were completely removed from zeolite, while removing only about 30 % of Cu.

#### 4. Conclusions

In this study, magnetic coal fly ash CFA-derived and magnetic LTA zeolites were used in a continuous flow system to assess their ability to adsorb Pb, Cu, Zn, and Ni from mixed ion solutions. Both magnetic zeolites (M-CFAZ and M-LTAZ) demonstrated the ability to remove metal ions at different flow rates and zeolite loadings, maintaining the selectivity order of Pb > Cu > Zn > Ni, consistent with findings from previous batch adsorption studies [33]. Thus, M-CFAZ removed 63 % Pb, 37 % Cu, 13 % Zn, and 7 % Ni whereas M-LTAZ removed 25 % Pb, 16 % Cu, 6 % Zn, and 3 % Ni, indicating better adsorption performance of M-CFAZ. Moreover, in both scenarios, the magnetic properties of the zeolite composites facilitated the complete capture of fine zeolite particles by the Wet High Intensity Magnetic Separator (WHIMS), ensuring that the treated solution is free from residual zeolite particulates. The results show that the type of zeolite affects the adsorption efficiency of the metals, with M-CFA zeolite generally outperforming M-LTA zeolite in terms of metal uptake. This feature enhances the practical and operational benefits of using magnetic synthetic zeolite in real-world

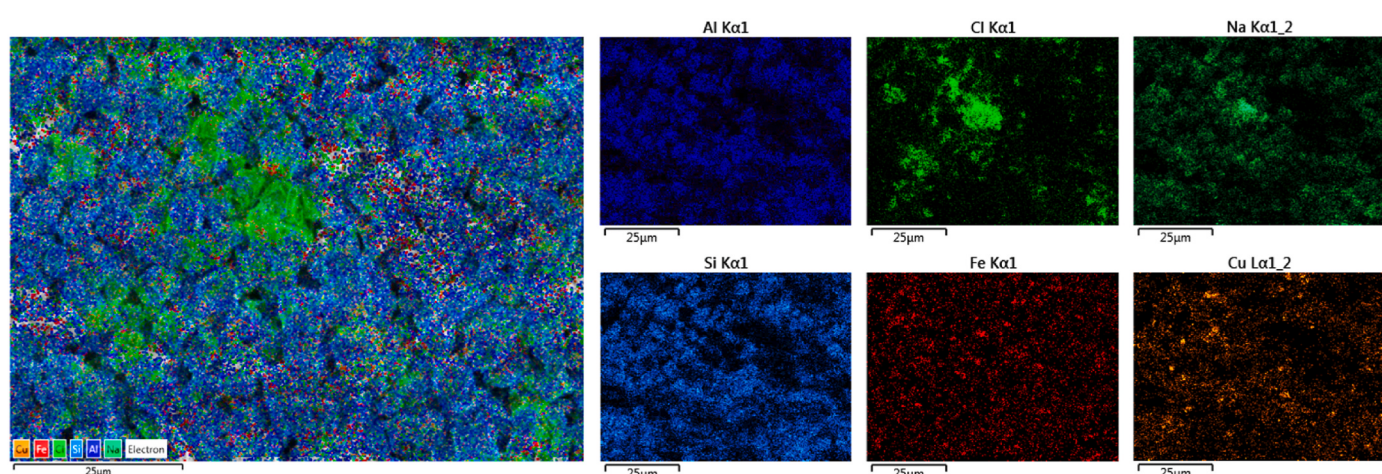


**Fig. 8.** SEM-EDS scans of M-CFA zeolite after desorption in NaCl solution showing the presence of Cu, Fe, Cl, Na, Si, and Al in the magnetic zeolite sample.

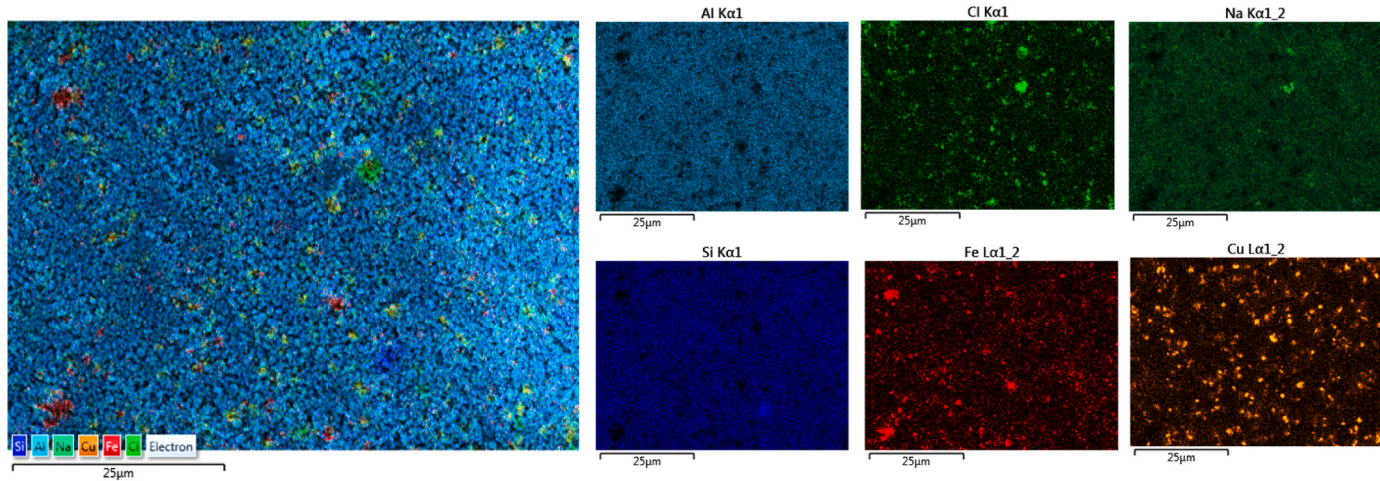


**Fig. 9.** SEM-EDS scans of M-LTA zeolite after desorption in NaCl solution showing the presence of Cu, Fe, Cl, Na, Si, and Al in magnetic zeolite sample.

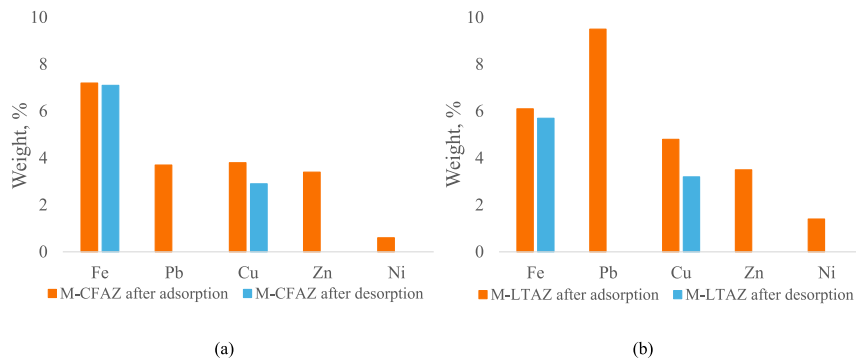


**Fig. 10.** EDS results of magnetic CFA zeolite (a) and magnetic LTA zeolite (b) after adsorption and after desorption experiments excluding zeolites constituents.

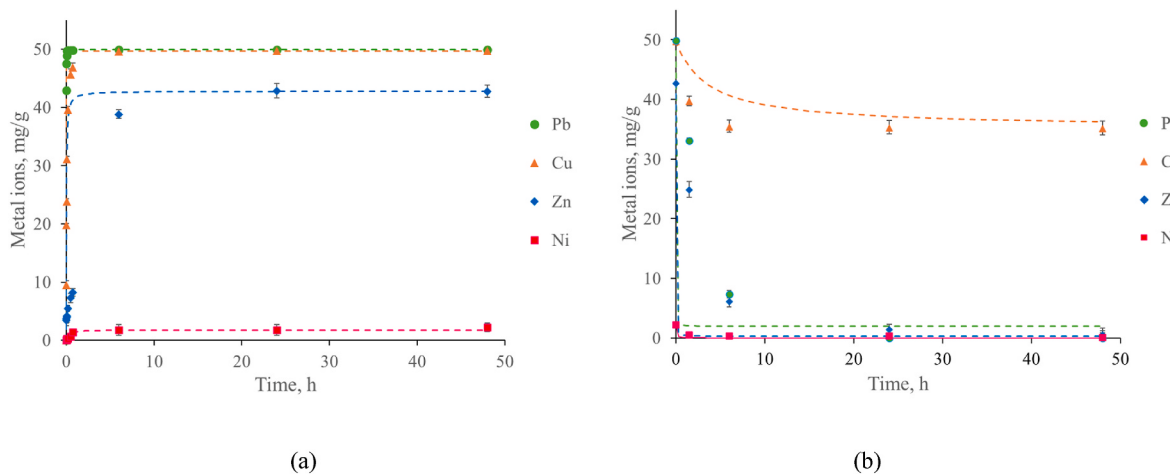


**Fig. 11.** Metal ion concentrations in M-CFAZ in mg/g zeolite measured over time during adsorption experiment (a) and desorption experiment (b). Curves are representation of pseudo-second-order adsorption model.

applications.

Desorption experiments were performed to clean the magnetic zeolite of metal ions using saturated NaCl solutions to facilitate ion exchange. Both solution and the zeolite surface were analyzed using ICP-OES and SEM-EDS techniques, respectively. The results indicated the removal of 100 % Pb, Zn, and Ni and 30 % of Cu from zeolite. It is possible that increasing the volume of the NaCl solution used for

desorption of metals from the zeolite would provide more Na<sup>+</sup> ions available for exchange with metal (M<sup>2+</sup>) ions and enhance Cu recovery. Another hypothesis is that the sites of the carbonized graphenic coke binder initially absorbed most of the Cu ions from the solution until these sites became saturated, after which the Cu ions began to adsorb onto the zeolite. When attempting to remove the Cu ions with a NaCl solution, only the Cu adsorbed on the zeolite is effectively desorbed,

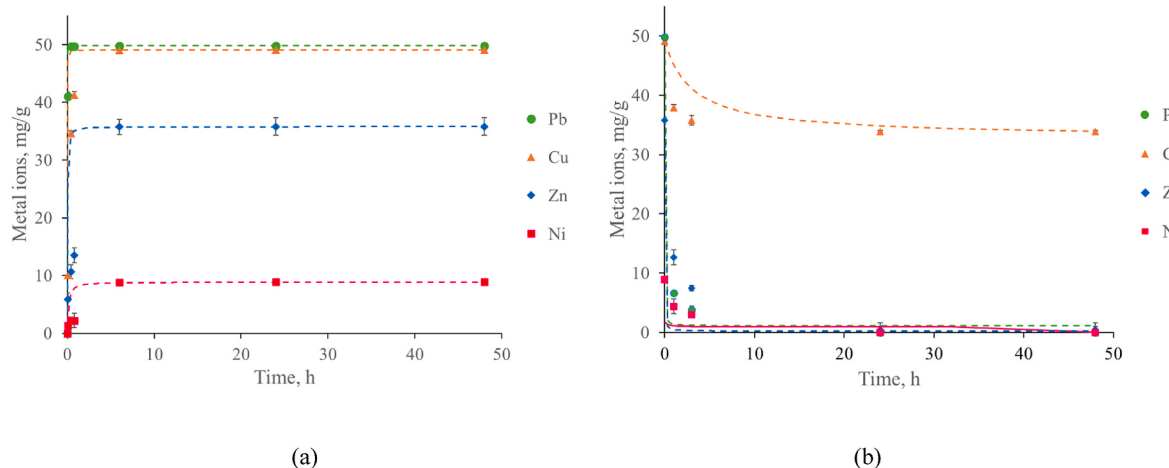


**Fig. 12.** Metal ion concentrations in M-LTAZ in mg/g zeolite measured over time during adsorption experiment (a), desorption experiment (b). The curves represent the pseudo-second-order adsorption model.

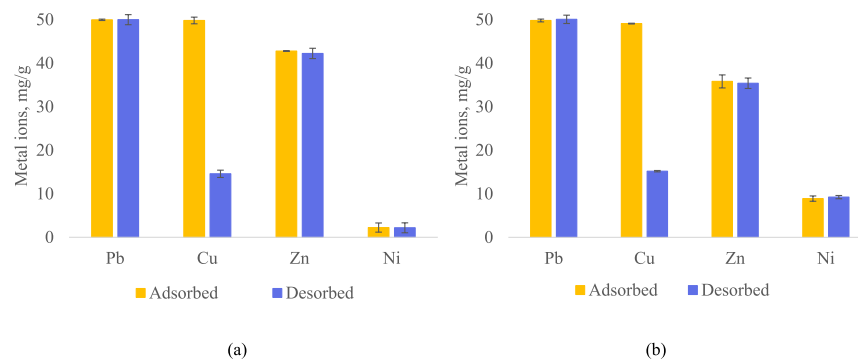


**Fig. 13.** Adsorbed and desorbed metal ions per g of M-CFAZ (a) and M-LTAZ (b).

**Table 6**  
Adsorbed and desorbed metal ions per g of M-CFAZ and M-LTAZ.

	M-CFAZ				M-LTAZ			
	Pb	Cu	Zn	Ni	Pb	Cu	Zn	Ni
Adsorbed, mg/g	50	50	43	2	50	49	36	9
Desorbed, mg/g	50	15	42	2	50	15	35	9

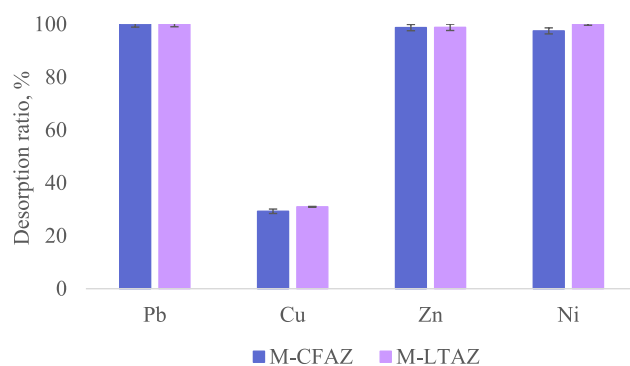


**Fig. 14.** Comparison of desorption ratio of M-CFAZ and M-LTAZ.

while the Cu retained in the graphenic sites of the binder remains unaffected by the NaCl solution which might be due the strong surface complexation of Cu ions with the oxygen-containing groups on the surface of graphene oxide [57]. Further investigation into this phenomenon would be of significant value, potentially uncovering new insights and deepening the knowledge of the underlying mechanisms and improve desorption efficiency and regeneration process for magnetic zeolites.

The study highlighted the relationship between metal ions in adsorption and desorption processes, showing the importance of ion competition in designing adsorption systems to treat solutions with multiple metal contaminants. Thus, the adsorption selectivity order was found as  $\text{Pb}^{2+} > \text{Cu}^{2+} > \text{Zn}^{2+} > \text{Ni}^{2+}$ , while in desorption experiments a different selectivity order was observed, with  $\text{Cu}^{2+}$  ions remaining in the sample while  $\text{Pb}^{2+}$ ,  $\text{Zn}^{2+}$  and  $\text{Ni}^{2+}$  were completely removed. These could be due to the difference in bond type and strength formed by metal ions with zeolite structure, as well as the difference in metal ions, including parameters such as molar weight, electric charge, and ionic radius among the different ions. Additionally, the regenerated magnetic zeolite shows promise for multiple reuses in subsequent water treatment cycles, thereby enhancing the sustainability of the process. When exhausted, metal-loaded zeolite can be incorporated into construction materials including concrete production [58–60]. It has been shown in several studies that zeolite not only adds structural properties but also immobilizes heavy metals, preventing environmental leaching [60,61]. Therefore, the proposed utilization of magnetic CFA-synthesized zeolite not only reduces CFA waste and treats industrial wastewater

contaminated with heavy metal ions, but also potentially streamlines the recycling and repurposing of the used zeolite, consequently mitigating environmental impacts.

Overall, the study demonstrated that the magnetic CFA-derived zeolite exhibits excellent potential for repeated adsorption-desorption cycles, showing its promise as a sustainable and reusable material for water treatment applications. However, while the initial results are highly encouraging, further comprehensive investigation to assess M-CFAZ long-term stability and performance over multiple operational cycles would be beneficial for validating its practicality and reliability for large-scale industrial applications.

### CRediT authorship contribution statement

**Sofi Buzukashvili:** Writing – review & editing, Writing – original draft, Methodology, Investigation, Formal analysis, Data curation. **Roberto Sommerville:** Writing – review & editing, Methodology, Formal analysis, Conceptualization. **Ozan Kökkilic:** Writing – review & editing, Methodology, Investigation, Formal analysis. **Philippe Ouzilleau:** Writing – review & editing, Methodology, Formal analysis, Conceptualization. **Neil A. Rowson:** Writing – review & editing, Methodology, Conceptualization. **Kristian E. Waters:** Writing – review & editing, Supervision, Resources, Project administration, Methodology, Funding acquisition, Conceptualization.

### Declaration of competing interest

The authors have declared no conflict of interest.

### Acknowledgements

The authors are grateful for the financial support from the Natural Sciences and Engineering Research Council of Canada (NSERC), Teck Resources Limited, COREM, SGS Canada Inc. and Flottet, under the Collaborative Research and Development Grants Program [grant number CRDPJ-531957-18]. The McGill Engineering Doctoral Award (MEDA) from the Faculty of Engineering at McGill University is also acknowledged for a scholarship awarded to S. Buzukashvili.

### Data availability

Data will be made available on request.

### References

- [1] D. Jassby, T.Y. Cath, H. Buisson, The role of nanotechnology in industrial water treatment, *Nat. Nanotechnol.* 13 (8) (2018) 670–672.
- [2] J. Ahmed, A. Thakur, A. Goyal, Industrial wastewater and its toxic effects, in: M.P. Shah (Ed.), *Biological Treatment of Industrial Wastewater*, The Royal Society of Chemistry2021, p. 420.
- [3] P. Babuji, S. Thirumalaisamy, K. Duraisamy, G. Periyasamy, Human health risks due to exposure to water pollution: a review, *Water* 15 (14) (2023) 2532.
- [4] A. Inyinbor Adejumoke, O. Adebesin Babatunde, P. Oluyori Abimbola, A. Adelani-Akande Tabitha, O. Dada Adewumi, A. Oreofe Toyin, Water pollution: effects, prevention, and climatic impact, in: G. Matjaž (Ed.), *Water Challenges of an Urbanizing World*, IntechOpen, Rijeka, 2018. Ch. 3.
- [5] L. Lin, H. Yang, X. Xu, Effects of water pollution on human health and disease heterogeneity: a review, *Front. Environ. Sci.* 10 (2022).
- [6] M.S. Lawan, R. Kumar, J. Rashid, M.A.E.-F. Barakat, Recent advancements in the treatment of petroleum refinery wastewater, *Water* 15 (20) (2023) 3676.
- [7] A. Azimi, A. Azari, M. Rezakazemi, M. Ansarpour, Removal of heavy metals from industrial wastewaters: a review, *ChemBioEng Rev.* 4 (1) (2017) 37–59.
- [8] S. Buzukashvili, R. Sommerville, N.A. Rowson, K.E. Waters, An overview of zeolites synthesised from coal fly ash and their potential for extracting heavy metals from industrial wastewater, *Can. Metall. Q.* 63 (1) (2023) 130–152.
- [9] M.A. Barakat, New trends in removing heavy metals from industrial wastewater, *Arab. J. Chem.* 4 (4) (2011) 361–377.
- [10] C. Zamora-Ledezma, D. Negrete-Bolagay, F. Figueroa, E. Zamora-Ledezma, M. Ni, F. Alexis, V.H. Guerrero, Heavy metal water pollution: a fresh look about hazards, novel and conventional remediation methods, *Environ. Technol. Innovat.* 22 (2021) 101504.
- [11] N.A.A. Qasem, R.H. Mohammed, D.U. Lawal, Removal of heavy metal ions from wastewater: a comprehensive and critical review, *npj Clean Water* 4 (1) (2021) 36.
- [12] S.P. Viswanathan, G.M. Kuriakose, S.P. Neelamurthy, G.V. Njazakunnathu, T. A. Paili, Biochar-based composites as environmentally sustainable functional materials for wastewater treatment. *Comprehensive Material Processing* Second Edition, 2, 2024, pp. 303–318.
- [13] F. Matebese, A.K. Mosai, H. Tutu, Z.R. Tshentu, Mining wastewater treatment technologies and resource recovery techniques: a review, *Heliyon* 10 (3) (2024) e24730.
- [14] F. Fu, Q. Wang, Removal of heavy metal ions from wastewaters: a review, *J. Environ. Manag.* 92 (3) (2011) 407–418.
- [15] D. Dutta, S. Arya, S. Kumar, Industrial wastewater treatment: current trends, bottlenecks, and best practices, *Chemosphere* 285 (2021) 131245.
- [16] S. Abdur Razzak, M.O. Faruque, Z. Alsiekh, L. Alsiekhmohamad, D. Alkuroud, A. Alfayez, S.M. Hossain, M. Hossain, A comprehensive review on conventional and biological-driven heavy metals removal from industrial wastewater, *Environ. Adv.* 7 (2022) 100168.
- [17] M.R. Silva, A. Lecus, M. Gajdardziska-Josifovska, M. Schofield, M. Virnoche, J. Chang, J. Chen, D. Garman, Graphene-oxide loading on natural zeolite particles for enhancement of adsorption properties, *RSC Adv.* 10 (8) (2020) 4589–4597.
- [18] M. Król, Natural vs. Synthetic zeolites, *Crystals* 10 (7) (2020) 622, 7.
- [19] A. Dyer, Chapter 16 - ion-exchange properties of zeolites and related materials, in: J. Čejka, H. van Bekkum, A. Corma, F. Schüth (Eds.), *Studies in Surface Science and Catalysis*, Elsevier2007, pp. 525–553.
- [20] A. Khaleque, M.M. Alam, M. Hoque, S. Mondal, J.B. Haider, B. Xu, M.A.H. Johir, A. K. Karmakar, J.L. Zhou, M.B. Ahmed, M.A. Moni, Zeolite synthesis from low-cost materials and environmental applications: a review, *Environ. Adv.* 2 (2020) 100019.
- [21] F. Collins, A. Rozhkovskaya, J.G. Outram, G.J. Millar, A critical review of waste resources, synthesis, and applications for Zeolite LTA, *Microporous Mesoporous Mater.* 291 (2020) 109667.
- [22] A. Julbe, M. Drobek, Zeolite A type, in: E. Drioli, L. Giorno (Eds.), *Encyclopedia of Membranes*, Springer, Berlin Heidelberg, Berlin, Heidelberg, 2016, pp. 2055–2056.
- [23] S. Gao, H. Peng, B. Song, J. Zhang, W. Wu, J. Vaughan, P. Zardo, J. Vogrin, S. Tulloch, Z. Zhu, Synthesis of zeolites from low-cost feeds and its sustainable environmental applications, *J. Environ. Chem. Eng.* 11 (1) (2023) 108995.
- [24] D. Chen, X. Hu, L. Shi, Q. Cui, H. Wang, H. Yao, Synthesis and characterization of zeolite X from lithium slag, *Appl. Clay Sci.* 59–60 (2012) 148–151.
- [25] Y. Chen, Y. Fan, Y. Huang, X. Liao, W. Xu, T. Zhang, A comprehensive review of toxicity of coal fly ash and its leachate in the ecosystem, *Ecotoxicol. Environ. Saf.* 269 (2024) 115905.
- [26] D. Harris, C. Heidrich, J. Feuerborn, *Global Aspects on Coal Combustion Products*, 2019.
- [27] A.Q. Vilakazi, S. Ndlovu, L. Chipise, A. Shemi, The recycling of coal fly ash: a review on sustainable developments and economic considerations, *Sustainability* 14 (4) (2022) 1958.
- [28] J.Z. Buha Marković, A.D. Marinković, J.Z. Savić, M.R. Mladenović, M.D. Erić, Z. J. Marković, M.D. Ristić, Risk evaluation of pollutants emission from coal and coal waste combustion plants and environmental impact of fly ash landfilling, *Toxics* 11 (4) (2023) 396.
- [29] Z. Asif, Z. Chen, H. Wang, Y. Zhu, Update on air pollution control strategies for coal-fired power plants, *Clean Technol. Environ. Policy* 24 (8) (2022) 2329–2347.
- [30] D. Harris, Ash as an internationally traded commodity, *Coal Combustion Products (CCP's)*, Elsevier2017, pp. 509–529.
- [31] M. Maharanan, S. Sen, Magnetic zeolite: a green reusable adsorbent in wastewater treatment, *Mater. Today: Proc.* 47 (2021) 1490–1495.
- [32] F. Younas, A. Mustafa, Z.U.R. Farooqi, X. Wang, S. Younas, W. Mohy-Ud-Din, M. Ashir Hameed, M. Mohsin Abrar, A.A. Maitlo, S. Noreen, M.M. Hussain, Current and emerging adsorbent technologies for wastewater treatment: trends, limitations, and environmental implications, *Water* 13 (2) (2021) 215.
- [33] S. Buzukashvili, R. Sommerville, W. Hu, O. Brooks, O. Kökkilic, P. Ouzilleau, N. A. Rowson, K.E. Waters, Zeolite synthesis from coal fly ash and its application to heavy metals remediation from water contaminated with Pb, Cu, Zn and Ni ions, *Miner. Eng.* 209 (2024).
- [34] S. Buzukashvili, W. Hu, R. Sommerville, O. Brooks, O. Kökkilic, N.A. Rowson, P. Ouzilleau, K.E. Waters, Magnetic zeolite: synthesis and copper adsorption followed by magnetic separation from treated water, *Crystals* 13 (9) (2023).
- [35] N. Ghosh, S. Sen, G. Biswas, A. Saxena, P.K. Halder, Adsorption and desorption study of reusable magnetic iron oxide nanoparticles modified with *Justicia adhatoda* leaf extract for the removal of textile dye and antibiotic, *Water, Air, Soil Pollut.* 234 (3) (2023) 202.
- [36] M. Wahajuddin, S. Arora, Superparamagnetic iron oxide nanoparticles: magnetic nanoplatforms as drug carriers, *Int. J. Nanomed.* 7 (2012) 3445–3471.
- [37] M. Gallegos-Garcia, K. Ramírez-Muñiz, S. Song, Arsenic removal from water by adsorption using iron oxide minerals as adsorbents: a review, *Miner. Process. Extr. Metall. Rev.* 33 (5) (2012) 301–315.
- [38] S.I. Siddiqui, S.A. Chaudhry, Iron oxide and its modified forms as an adsorbent for arsenic removal: a comprehensive recent advancement, *Process Saf. Environ. Protect.* 111 (2017) 592–626.
- [39] N.N. Nassar, Iron oxide nanoadsorbents for removal of various pollutants from wastewater: an overview. *Application of Adsorbents for Water Pollution Control*, 2012, pp. 81–118.
- [40] J. Liu, Y. Yu, S. Zhu, J. Yang, J. Song, W. Fan, H. Yu, D. Bian, M. Huo, Synthesis and characterization of a magnetic adsorbent from negatively-valued iron mud for methylene blue adsorption, *PLoS One* 13 (2) (2018) e0191229.

- [41] J. Zhu, S. Wei, M. Chen, H. Gu, S.B. Rapole, S. Pallavkar, T.C. Ho, J. Hopper, Z. Guo, Magnetic nanocomposites for environmental remediation, *Adv. Powder Technol.* 24 (2) (2013) 459–467.
- [42] R. Thompson, K. Franklin, in: H. Robson, K.P. Lillerud (Eds.), Chapter 55—LTA Linde Type A Si (50), Al (50), *Verified Syntheses of Zeolitic Materials*, 2001, pp. 179–181.
- [43] R. Sommerville, R. Blissett, N. Rowson, S. Blackburn, Producing a synthetic zeolite from improved fly ash residue, *Int. J. Miner. Process.* 124 (2013) 20–25.
- [44] R.P.Z. Sommerville, *Utilisation of Fly Ash in the Manufacture of Zeolites*, School of Chemical Engineering, University of Birmingham, 2017.
- [45] S. Mintova, *Verified syntheses of zeolitic materials*, Synthesis Commission of the International Zeolite Association2016.
- [46] The International Zeolite Association. Database of zeolite structures. [https://america.iza-structure.org/IZA-SC/ftc\\_table.php](https://america.iza-structure.org/IZA-SC/ftc_table.php). (Accessed May 2024).
- [47] R.C.F. de Lima, D.d.S. Oliveira, S.B.C. Pergher, Interzeolitic transformation of clinoptilolite into GIS and LTA zeolite, *Minerals* 11 (12) (2021) 1313.
- [48] T.B. Reed, D.W. Breck, Crystalline zeolites. II. Crystal structure of synthetic zeolite, type A, *J. Am. Chem. Soc.* 78 (23) (1956) 5972–5977.
- [49] A.R. Loiola, J.C.R.A. Andrade, J.M. Sasaki, L.R.D. da Silva, Structural analysis of zeolite NaA synthesized by a cost-effective hydrothermal method using kaolin and its use as water softener, *J. Colloid Interface Sci.* 367 (1) (2012) 34–39.
- [50] R.M. Mohamed, A.A. Ismail, G. Kini, I.A. Ibrahim, B. Koopman, Synthesis of highly ordered cubic zeolite A and its ion-exchange behavior, *Colloids Surf. A Physicochem. Eng. Asp.* 348 (1) (2009) 87–92.
- [51] X. Pan, G. Zuo, T. Su, S. Cheng, Y. Gu, X. Qi, W. Dong, Polycarboxylic magnetic polydopamine sub-microspheres for effective adsorption of malachite green, *Colloids Surf. A Physicochem. Eng. Asp.* 560 (2019) 106–113.
- [52] W.J.J. Weber, J.C. Morris, Kinetics of adsorption on carbon from solution, *J. Sanit. Eng. Div.* 89 (1963) 31–59.
- [53] M. Musah, Y. Azeb, J. Mathew, M. Umar Tanko, Z. Abdulhamid, A. Muhammad, Adsorption kinetics and isotherm models: a review, *Caliphate J. Sci. Technol.* 4 (2022).
- [54] J.-Y. Tseng, C.-Y. Chang, C.-F. Chang, Y.-H. Chen, C.-C. Chang, D.-R. Ji, C.-Y. Chiu, P.-C. Chiang, Kinetics and equilibrium of desorption removal of copper from magnetic polymer adsorbent, *J. Hazard Mater.* 171 (1) (2009) 370–377.
- [55] J. Wang, X. Guo, Adsorption kinetic models: physical meanings, applications, and solving methods, *J. Hazard Mater.* 390 (2020) 122156.
- [56] N. Öztaş, A. Karabakan, Ö. Topal, Removal of Fe (III) ion from aqueous solution by adsorption on raw and treated clinoptilolite samples, *Microporous Mesoporous Mater.* 111 (1–3) (2008) 200–205.
- [57] R. Sitko, E. Turek, B. Zawisza, E. Malicka, E. Talik, J. Heimann, A. Gagor, B. Feist, R. Wrzalik, Adsorption of divalent metal ions from aqueous solutions using graphene oxide, *Dalton Trans.* 42 (16) (2013) 5682–5689.
- [58] A. V. R. Cioffi, P. Michele, C. C. Disposal of lead-containing zeolite sludges in cement matrix, *Environ. Technol.* 16 (1995) 147–156.
- [59] G. Girskas, I. Pundziene, J. Pranckevicienė, The effect of natural and synthesised zeolites on cement-based materials hydration and hardened state properties, *Materials* 16 (16) (2023).
- [60] X. Lu, F. Wang, X.-y. Li, K. Shih, E.Y. Zeng, Adsorption and thermal stabilization of Pb<sup>2+</sup> and Cu<sup>2+</sup> by zeolite, *Ind. Eng. Chem. Res.* 55 (32) (2016) 8767–8773.
- [61] N. Kordala, M. Wyszkowski, Zeolite properties, methods of synthesis, and selected applications, *Molecules* 29 (5) (2024) 1069.